

Constrained and Regularized Quantitative Ultrasound Parameter Estimation using ADMM

Ali K. Z. Tehrani¹, Hassan Rivaz¹, and Ivan M. Rosado-Mendez²

¹Department of Electrical and Computer Engineering, Concordia University, Canada.

Email: ali.kafaeizadtehrani@mail.concordia.ca, hrivaz@ece.concordia.ca.

²Department of Medical Physics and Radiology, University of Wisconsin, United States.

Email: rosadomendez@wisc.edu.

Abstract

Regularized estimation of quantitative ultrasound (QUS) parameters, such as attenuation and backscatter coefficients, has gained research interest. Recently, the alternating direction method of multipliers (ADMM) has been applied successfully to estimate these parameters, by utilizing L2 and L1 norms for attenuation and backscatter coefficient regularization, respectively. While this method improves upon previous approaches, it does not fully leverage the prior knowledge of minimum physically feasible parameter values, sometimes yielding values outside the realistic range. This work addresses this limitation by incorporating minimum QUS parameter values as constraints to enhance ADMM estimation. The proposed method is validated using experimental phantom data.

1 Introduction

Quantitative ultrasound (QUS) reveals the quantitative properties of the tissue microstructure [1–3], and have been extensively utilized in breast cancer diagnosis [4, 5], fatty liver disease classification [6], and prostate cancer monitoring [7]. Spectral-based QUS methods employ RF data backscattered from the tissue to estimate different parameters such as attenuation coefficient, backscattering coefficient (BSC), and effective scatterer diameter (ESD) [8–11]. In this work, we focus on estimating the attenuation coefficient and BSC from the power spectra.

Several approaches have been proposed to estimate the mentioned parameters. Reference phantom model (RPM) is a well-known method used to cancel the system-dependant effects [12]. A reference phantom imaged by the same imaging setting was utilized to

remove system-dependent effects. The RPM employs least squares optimization, leading to high variance in parameter estimation. In [13], dynamic programming was introduced to account for the dependency between neighboring samples, incorporating regularization to mitigate variance. Another method, Analytical Globally Regularized Backscatter Quantitative Ultrasound (ALGEBRA), optimizes a penalty function with L2 norm regularization terms [14]. More recently, the Alternating Direction Method of Multipliers (ADMM) has been suggested to overcome the limitations of ALGEBRA, such as relying on the L2 norm for both attenuation and BSC, assigning equal importance to all frequencies, and reduced performance in the presence of specular reflectors [15]. This work presents a modification to the ADMM solution to incorporate prior knowledge of the minimum value of the estimated parameters as a constraint in the optimization framework.

2 Material and Methods

2.1 Problem formulation

Based on RPM, the power spectra are divided by the power spectra of a reference phantom with known parameters to remove system-dependant effects, which yields [12–15]:

$$\frac{S_t(x, z, f)}{S_r(x, z, f)} = \frac{\sigma_t(x, z, f)A_t(x, z, f)}{\sigma_r(x, z, f)A_r(x, z, f)} \quad (1)$$

where x , z , and f denote the lateral position, depth, and frequency, respectively, and the subscripts t and r represent the target and reference phantom. The system-independent power spectra are modeled as a multiplication of the BSC (σ) and total attenuation

(A), which can be defined for the target as [12–15]:

$$\begin{aligned}\sigma_t(z, f) &= b_t(z) f^{n_t} \\ A_t(z, f) &= \exp(-4\overline{\alpha}_t f z)\end{aligned}\quad (2)$$

by taking the natural logarithm and applying (2) into (1) we can obtain:

$$\begin{aligned}X(f, z) &= b + n \ln f - 4\alpha f z \\ \ln \frac{b_t}{b_r} &\equiv b, \quad n_t - n_r \equiv n, \quad \overline{\alpha}_t - \overline{\alpha}_r \equiv \alpha\end{aligned}\quad (3)$$

The goal is to estimate b , n , and α from the observed $X(f, z)$.

2.2 ADMM method

Jafarpisheh *et al.* proposed using ADMM optimizer to estimate the QUS parameters. They used L2 norm regularization for α since it has gradual variations and employed L1 norm regularization for BSC since it can have abrupt changes [15]. They also utilized adaptive weights for different frequencies since the importance of different frequencies may change with depth and SNR.

Explaining the details of how the ADMM solution has been derived is out of scope of this work but the final results are given here. The algorithm tries to minimize the following constrained cost function:

$$\begin{aligned}C &= \frac{1}{2} \|Hx - t\|_2^2 + \lambda_1 \|s_1\|_2^2 + \lambda_2 \|s_2\|_1 \\ \text{s.t.} \quad K_1 x_1 - s_1 &= 0, \quad K_2 x_2 - s_2 = 0.\end{aligned}\quad (4)$$

where x is the vector containing b , n , α of all samples in a line, $x = \{\alpha_1, \alpha_2, \dots, \alpha_{N_R}, b_1, b_2, \dots, b_{N_R}, n_1, n_2, \dots, n_{N_R}\}^T$, and N_R denotes the number of samples in a line. H is a known transformation matrix (refer to [15] for more details), and t is the observed power spectra sample. The x_1 is part of x containing only α values, x_2 is the part containing b and n values; and K_1 , and K_2 denote the regularization weight matrices. By adding the latent variables, (4) can be converted to an unconstrained cost function, and ADMM update rules can be derived as:

$$\begin{aligned}x^{k+1} &:= (H^T H + \rho K^T K)^{-1} H^T t + \rho K^T (s^k - y^k) \\ s_1^{k+1} &:= (K_1 x_1^{k+1} + y_1^k) / (\rho + \lambda_1) \\ s_2^{k+1} &:= S_{\lambda_2/\rho} (K_2 x_2^{k+1} + y_2^k) \\ y^{k+1} &:= y^k + K x^{k+1} - s^{k+1}\end{aligned}\quad (5)$$

where $S_{\frac{\lambda}{\rho}} = \text{sgn}(\cdot) \max\left\{|\cdot| - \frac{\lambda}{\rho}, 0\right\}$ performs soft thresholding.

2.3 Proposed method

The ADMM approach incorporates the regularization of L1 and L2 norms, but it does not utilize any constraint regarding the feasible range of the estimated variables. In this work, we incorporate the minimum physically feasible values as the constraints to provide prior knowledge to the cost function. The new constrained optimization cost function can be written as [16]:

$$\begin{aligned}C &= \frac{1}{2} \|Hx - t\|_2^2 + \lambda_1 \|s_1\|_2^2 + \lambda_2 \|s_2\|_1 \\ \text{s.t.} \quad K_1 x_1 - s_1 &= 0, \quad K_2 x_2 - s_2 = 0. \\ \Phi x - v &= \beta\end{aligned}\quad (6)$$

The last phrase is added to represent the minimum value constraint, where

$\beta = [\alpha_{m_1}, \dots, \alpha_{m_{N_R}}, b_{m_1}, \dots, b_{m_{N_R}}, n_{m_1}, \dots, n_{m_{N_R}}]^T$ is the vector containing the minimum feasible values for each parameter, v denotes the new latent variable added to facilitate the incorporation of the constraint, and Φ is an identity matrix. We considered that the attenuation ($\overline{\alpha}_t$), BSC (b_t), and n_t are greater than 0, 0.001 of the reference and 0, respectively. Therefore, the minimum values (α_m , b_m , and n_m) can be obtained as:

$$b_m \equiv \ln(0.001), \quad n_m \equiv -n_r, \quad \alpha_m \equiv -\overline{\alpha}_r \quad (7)$$

The constrained optimization in 6 can be converted into an unconstrained optimization problem by adding a latent variable (called q here), and the update rule can be written as [16]:

$$\begin{aligned}x^{k+1} &:= (H^T H + \rho K^T K)^{-1} H^T t \\ &\quad + \rho K^T (s^k - y^k) + \gamma \phi^T (v^k - q^k) \\ v^{k+1} &= \text{clip}\{x^{k+1} + q, \beta\} \\ q^{k+1} &= q^k + (x^{k+1} - v^{k+1}) \\ S_1^{k+1} &= \frac{K_1 x_1^{k+1} + y_1}{\rho + \lambda_1} \\ S_2^{k+1} &= S_2 (K_2 x_2 + y_2) \\ y &= y + K x^{k+1} - S\end{aligned}\quad (8)$$

The clip function ensures that v stays higher than the minimum physically feasible value (β), and the latent variable q tries to make the estimated variables (x) as close as possible to v . We named this method Constrained-ADMM (C-ADMM), and γ is a hyper-parameter that should be tuned for each application.

2.4 Datasets

2.4.1 Phantom With Specular Reflectors

We employed Verasonics Vantage 128 system (Verasonics, Kirkland, WA, USA) with an L11-5v transducer operating at 8 MHz to collect data from Gammex 410 SCG phantom (Gammex-Sun Nuclear, Middleton, WI, USA, serial number 805546-4612). There are nylon filaments to produce specular reflection, and the transducer aperture was aligned with the long axis of the fibers. The phantom has $\bar{\alpha}_t = 0.6035 \text{ dB cm}^{-1} \text{ MHz}^{-1}$, $b_t = 2.996 \times 10^{-6} \text{ cm}^{-1} \text{ sr}^{-1}$, and $n_t = 3.428$. The B-mode image of this phantom is depicted in Fig. 1. The main interest is estimating the QUS parameters of the background in the presence of reflectors to investigate how the reflectors affect the estimation of the background QUS parameters.

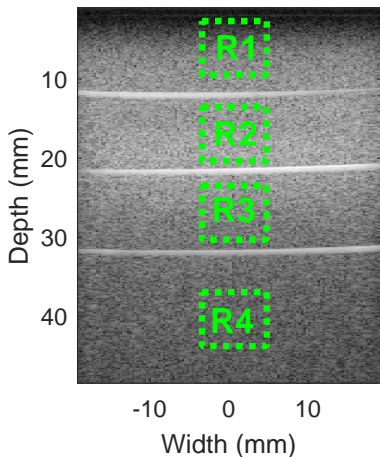


Figure 1: The B-mode image of the phantom.

2.5 Quantitative metrics

We report the bias error and variance of the estimated parameters, which can be defined as:

$$\text{bias} = E\{|\theta - \theta_{gt}|\}, \quad \text{Variance} = E\{(\theta - \theta_{gt})^2\} \quad (9)$$

where θ is the estimated parameter, and $E(\cdot)$ denotes averaging within the ROI. We report the bias and variance of BSC in dB scale. The results are reported for the four regions of size $5 \times 6 \text{ mm}$ highlighted in Fig. 1.

3 Results

Figure 2 shows the estimated attenuation coefficient map (A), BSC in dB (B), and n_t (C) using ADMM,

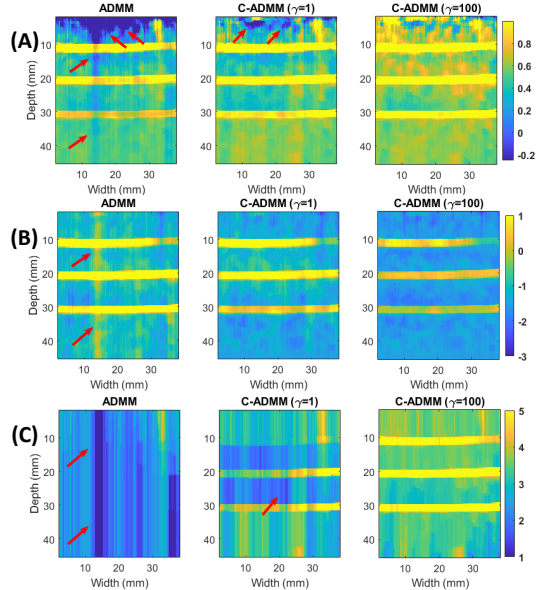


Figure 2: QUS parameter estimation results. α_t : Attenuation Coefficient (A), b_t : Backscattering Coefficient in dB (B), and n_t : frequency dependency (C). The marked area with red arrows illustrates the region where there are artifacts.

the proposed C-ADMM with $\gamma = 1$, and $\gamma = 100$. The red arrows illustrate the region where there is a large error. ADMM has a high error in depths lower than 10 mm for the attenuation coefficient, giving negative values that are not physically feasible. Furthermore, an incorrect band is visible in all three estimated parameters by ADMM. The proposed C-ADMM with $\gamma = 100$ does not estimate negative values for the attenuation coefficient, and the incorrect band has been removed. It should also be noted that ADMM fails to correctly calculate n_t (C) in all regions. However, C-ADMM obtains a more reliable estimate of this parameter. Comparing the C-ADMM with $\gamma = 1$ and $\gamma = 100$, C-ADMM with $\gamma = 100$ outperforms C-ADMM with $\gamma = 1$ (artifacts are marked in C-ADMM with $\gamma = 1$ by red arrows).

The bias errors for different regions specified in Fig. 1 are presented in Fig. 3, 4 and 5 for the attenuation coefficient, BSC, and n_t , respectively. As shown in Fig. 3, region R1 exhibits a substantial bias error, particularly with the ADMM method. However, C-ADMM significantly reduces this bias error, providing estimates that are much closer to the ground truth in this region. Additionally, for BSC and n_t , ADMM consistently shows high bias error across all regions. When comparing the hyper-parameter γ values, C-ADMM with $\gamma = 100$ achieves considerably lower bias error than with $\gamma = 1$,

Table 1: Variance of the estimated parameters

Method	α_t				b_t				n_t			
	R1	R2	R3	R4	R1	R2	R3	R4	R1	R2	R3	R4
ADMM	0.343	0.018	0.007	0.002	10.635	13.770	7.970	11.098	0.408	0.358	0.358	0.358
C-ADMM ($\gamma = 1$)	0.074	0.009	0.001	0.002	4.918	7.067	4.080	2.369	0.071	0.062	0.028	0.118
C-ADMM ($\gamma = 100$)	0.076	0.013	0.004	0.001	1.700	1.461	1.061	0.663	0.016	0.047	0.037	0.050

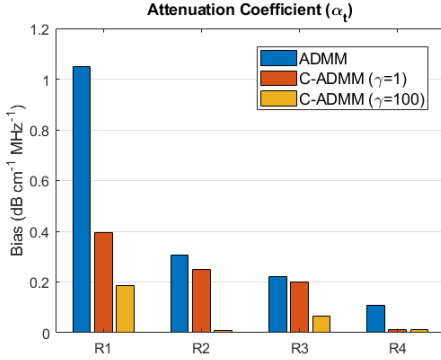


Figure 3: Attenuation Coefficient (α_t) bias error.

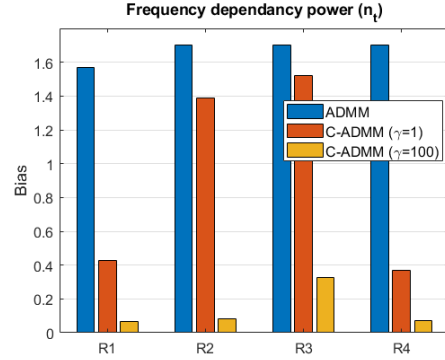


Figure 5: Frequency dependency power (n_t) bias error.

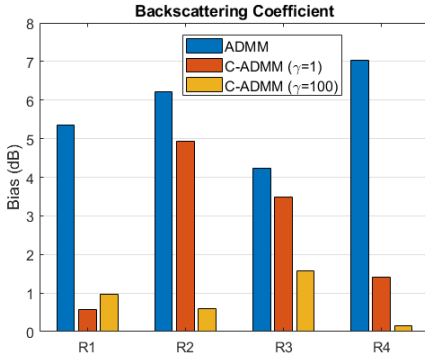


Figure 4: Backscattering Coefficient (b_t) bias error.

indicating that $\gamma = 100$ is a more optimal choice.

The variance of the estimated parameters is reported for different regions in Table 1. We can see a high variance in the attenuation coefficient estimated by ADMM in R1 (0.343), while C-ADMM has a considerably lower variance in this region (0.074 and 0.076). Furthermore, C-ADMM exhibits much lower variance for both BSC (b_t) and n_t compared to ADMM, which showcases it as a more reliable method than ADMM.

4 Discussion

We should note that in [15], the presented results of ADMM are averaged across multiple frames which further reduces the error. Here, we did not perform any

averaging across different frames, and utilizing multiple frames further improves the accuracy of the estimated parameters. We utilized a smaller patch size compared to [15] to better highlight the impact of the proposed method.

Another point is that the main aim of investigating the phantom with reflectors was to estimate the QUS parameters of the background in the presence of specular reflectors. We did not aim to estimate the parameters for the specular reflectors.

5 Conclusion

This work introduced C-ADMM, a modification of ADMM that incorporates minimum value constraints to integrate prior knowledge into the optimization framework. The proposed approach demonstrated improved parameter estimation, particularly in regions where ADMM struggled to yield physically feasible values due to noise and artifacts.

6 Acknowledgment

We acknowledge the support of Government of Canada’s New Frontiers in Research Fund (NFRF), [NFRFE-2022-00295] and Natural Sciences and Engineering Research Council of Canada (NSERC).

References

- [1] Michael L Oelze and Jonathan Mamou, “Review of quantitative ultrasound: Envelope statistics and backscatter coefficient imaging and contributions to diagnostic ultrasound,” *IEEE transactions on ultrasonics, ferroelectrics, and frequency control*, vol. 63, no. 2, pp. 336–351, 2016.
- [2] Ali KZ Tehrani, Mina Amiri, Ivan M Rosado-Mendez, Timothy J Hall, and Hassan Rivaz, “Ultrasound scatterer density classification using convolutional neural networks and patch statistics,” *IEEE Transactions on Ultrasonics, Ferroelectrics, and Frequency Control*, vol. 68, no. 8, pp. 2697–2706, 2021.
- [3] Ali KZ Tehrani, Ivan M Rosado-Mendez, and Hassan Rivaz, “Robust scatterer number density segmentation of ultrasound images,” *IEEE Transactions on Ultrasonics, Ferroelectrics, and Frequency Control*, vol. 69, no. 4, pp. 1169–1180, 2022.
- [4] Karina Quiaoit, Daniel DiCenzo, Kashuf Fatima, Divya Bhardwaj, Lakshmanan Sannachi, Mehrdad Gangeh, Ali Sadeghi-Naini, Archya Dasgupta, Michael C Kolios, Maureen Trudeau, et al., “Quantitative ultrasound radiomics for therapy response monitoring in patients with locally advanced breast cancer: Multi-institutional study results,” *PLoS One*, vol. 15, no. 7, pp. e0236182, 2020.
- [5] Mawia Khairalseed and Kenneth Hoyt, “High-resolution ultrasound characterization of local scattering in cancer tissue,” *Ultrasound in medicine & biology*, vol. 49, no. 4, pp. 951–960, 2023.
- [6] Trong Nguyen and Michael Oelze, “Reference free quantitative ultrasound classification of fatty liver,” in *2019 IEEE International Ultrasonics Symposium (IUS)*. IEEE, 2019, pp. 2424–2427.
- [7] Daniel Rohrbach, Brian Wodlinger, Jerrold Wen, Jonathan Mamou, and Ernest Feleppa, “High-frequency quantitative ultrasound for imaging prostate cancer using a novel micro-ultrasound scanner,” *Ultrasound in medicine & biology*, vol. 44, no. 7, pp. 1341–1354, 2018.
- [8] MF Insana and TJ Hall, “Characterising the microstructure of random media using ultrasound,” *Physics in Medicine & Biology*, vol. 35, no. 10, pp. 1373, 1990.
- [9] María Luisa Montero, Roberto Lavarello, and Andres Coila, “Simultaneous estimation of the nonlinearity parameter and attenuation coefficient with the gauss-newton levenberg-marquardt algorithm,” in *2024 IEEE Ultrasonics, Ferroelectrics, and Frequency Control Joint Symposium (UFFC-JS)*. IEEE, 2024, pp. 1–4.
- [10] Andres L Coila and Roberto Lavarello, “Regularized spectral log difference technique for ultrasonic attenuation imaging,” *IEEE transactions on ultrasonics, ferroelectrics, and frequency control*, vol. 65, no. 3, pp. 378–389, 2017.
- [11] Ping Gong, Pengfei Song, Chengwu Huang, Joshua Trzasko, and Shigao Chen, “System-independent ultrasound attenuation coefficient estimation using spectra normalization,” *IEEE transactions on ultrasonics, ferroelectrics, and frequency control*, vol. 66, no. 5, pp. 867–875, 2019.
- [12] Lin Xin Yao, James A Zagzebski, and Ernest L Madsen, “Backscatter coefficient measurements using a reference phantom to extract depth-dependent instrumentation factors,” *Ultrasonic imaging*, vol. 12, no. 1, pp. 58–70, 1990.
- [13] Zara Vajihi, Ivan M Rosado-Mendez, Timothy J Hall, and Hassan Rivaz, “Low variance estimation of backscatter quantitative ultrasound parameters using dynamic programming,” *IEEE transactions on ultrasonics, ferroelectrics, and frequency control*, vol. 65, no. 11, pp. 2042–2053, 2018.
- [14] Noushin Jafarpisheh, Timothy J Hall, Hassan Rivaz, and Ivan M Rosado-Mendez, “Analytic global regularized backscatter quantitative ultrasound,” *IEEE transactions on ultrasonics, ferroelectrics, and frequency control*, vol. 68, no. 5, pp. 1605–1617, 2020.
- [15] Noushin Jafarpisheh, Laura Castaneda-Martinez, Hayley Whitson, Ivan M Rosado-Mendez, and Hassan Rivaz, “Physics-inspired regularized pulse-echo quantitative ultrasound: Efficient optimization with admm,” *IEEE Transactions on Ultrasonics, Ferroelectrics, and Frequency Control*, 2023.
- [16] Gregory T Buzzard, Stanley H Chan, Suhas Sreehari, and Charles A Bouman, “Plug-and-play unplugged: Optimization-free reconstruction using consensus equilibrium,” *SIAM Journal on Imaging Sciences*, vol. 11, no. 3, pp. 2001–2020, 2018.